ARTICLE NO. 80-0272R

One- and Two-Phase Nozzle Flows

I-Shih Chang*
The Aerospace Corporation, El Segundo, Calif.

A time-dependent technique, in conjunction with the boundary-fitted coordinates system, is applied to solve a gas-only, one-phase inviscid flow and a fully coupled, gas-particle, two-phase inviscid flow inside nozzles with small throat radii of curvature, steep wall gradients, and submerged configurations. The emphasis of the study has been placed on one- and two-phase inviscid flow in the transonic region. Various particle sizes and particle mass fractions have been investigated in the two-phase flow. The salient features associated with the two-phase nozzle flow compared with those of the one-phase flow are illustrated through the calculations of the JPL nozzle, the Titan III solid rocket motor, and the submerged nozzle configuration found in the inertial upper stage (IUS) solid rocket motor.

Nomenclature

a = dimensionless local sonic speed, $a=\sqrt{T(\gamma-1)/2}$
A = exponent in the viscosity-temperature equation (7)
A_j = dimensionless friction term defined in Eq. (2)
B_j = dimensionless energy exchange term defined in Eq. (3)
C_D = drag coefficient
$\tilde{C}_j$ = particle heat capacity
$\tilde{C}_p$ = gas specific heat at constant pressure
e = dimensionless gas total energy per unit volume
$\tilde{E},\tilde{F},\tilde{G},\tilde{H}$ = vectors defined in Eq. (1)
E,F,G,H = vectors defined in Eq. (8)
f_j = momentum transfer parameter defined in Eq. (4)
g_c,g_r = convective and radiative parameters defined in Eq. (3)
h_j = dimensionless particle total energy per unit volume
J = Jacobian of transformation
$\tilde{L}$ = reference length scale, e.g., unit foot or unit meter
M = gas-phase Mach number
$\tilde{m}_j$ = particle mass density
N = index, $N=1$, one-phase gas-only flow; $N=2$, two-phase flow
Nu_j = particle Nusselt number
p = dimensionless pressure
Pr = gas-phase Prandtl number
q,q_j = dimensionless gas- and particle-phase speeds, respectively
r = dimensionless radial coordinate
$\tilde{r}_j$ = particle radius
Re_j = particle Reynolds number defined in Eq. (6)
t = dimensionless time, $t=\tilde{V}_{\max 1}\tilde{t}/\tilde{L}$
T,T_j = dimensionless gas- and particle-phase temperatures, respectively
u,u_j = dimensionless gas- and particle-phase horizontal velocity components, respectively
v,v_j = dimensionless gas- and particle-phase radial velocity components, respectively
$\tilde{V}_{\max 1}$ = adiabatic maximum speed evaluated at the inlet plane
W_j/W_m = particle mass fraction
x = dimensionless horizontal coordinate
γ = gas specific heat ratio
δ = geometric index, $\delta=0$, two dimension; $\delta=1$, axisymmetry
ϵ = gas emissivity
ϵ_j = particle emissivity
ζ = transformed dimensionless horizontal coordinate
λ_v = initial velocity lag, $\lambda_v=v_j/v$
λ_T = initial temperature ratio, $\lambda_T=T/T_j$
$\tilde{\mu}_g$ = gas viscosity
$\tilde{\mu}_{t1}$ = gas viscosity at stagnation state
ξ = transformed dimensionless radial coordinate
ρ = dimensionless gas density
ρ_j = dimensionless particle density
$\tilde{\sigma}$ = Stefan-Boltzmann constant
τ = $(\gamma-1)/2\gamma$
ϕ = particle mass fraction, $\phi=W_j/W_m$
ω = $\tilde{C}_j/\tilde{C}_p$

Superscripts

$(\vec{\ })$ = vectored quantity
$(\tilde{\ })$ = dimensioned quantity

Subscripts

g = gas phase
j = particle phase
m = mixture
$\max 1$ = maximum state evaluated at the inlet plane
$t1$ = stagnation state evaluated at the inlet plane

Received Dec. 3, 1979; presented as Paper 80-0272 at the AIAA 18th Aerospace Sciences Meeting, Pasadena, Calif., Jan. 14-16, 1980; revision received March 25, 1980.

Index categories: Nozzle and Channel Flow; Multiphase Flows; Transonic Flow.

*Member of Technical Staff, Aerothermodynamics Office. Member AIAA.

Introduction

THE nozzle and chamber flow analysis constitutes one of the important phases of aerospace research development work, since the performance of many vehicles relies on the rocket nozzle design. The classic analytical solution technique based upon the series expansion has limited application, as it requires the nozzle entrance to be suitably shaped. During the past decade the use of computers for the solution of nozzle flowfields[1,2] has been very popular among research engineers, mainly because the modern high-performance propulsion system, for the sake of length and weight reduction, usually possesses a nozzle contour with a small throat radius of curvature, a very steep wall gradient in the entrance region, or a submerged configuration, and the numerical technique is well suited for application to different nozzle geometric configurations. For gas-only, one-phase nozzle flows, various

numerical methods used in the past were reviewed in Ref. 2.

For the solid rocket motor, one of the prime causes of performance loss and surface damage is the presence of condensed metallic oxide particles of the combustion products in the flowfield. The thermal and velocity lag associated with the particles often result in decreased nozzle efficiency and degradation of the motor's effectiveness in converting from thermal to kinetic energy. Hence, knowledge of the role played by the nongaseous combustion products in the rapid expansion through the throat region and the qualitative estimation of this influence are essential in the design of a thrust nozzle. A comprehensive review of the investigation involving the gas-particle nozzle flowfield before 1962 is presented in Ref. 3. More recent studies include the numerical iterative relaxation technique of Ref. 4 and an uncoupled flow model described in Ref. 5. While the analysis used in these studies is helpful in explaining some of the physical processes involved in the gas-particle flows in the transonic region, both suffer from the same weakness: i.e., the assumption of the fixed gas-phase streamline coordinates. This is not necessarily true in a nozzle with very small throat radius of curvature or very steep wall gradient, since the presence of particles can alter the gas flow behavior. The constant fractional lag and the linear velocity profile assumptions used in Ref. 6 are not justified a priori. The results obtained or refined from a similar analysis for the transonic region[7] are highly uncertain, although they are the most widely used method in the propulsion industry.

In this paper, the time-dependent method is applied to the solution of gas-only, one-phase inviscid flow and fully coupled, gas-particle, two-phase inviscid flow inside nozzles of arbitrary geometry. The finite difference scheme and the inlet boundary conditions incorporated into the flowfield program are shown to yield good resolution of the entire subsonic-transonic-supersonic flow region. Moreover, to eliminate the computational difficulty associated with a nozzle with very steep wall or of a submerged configuration, the boundary-fitted coordinates (BFC) system[8] is adopted for generating a natural grid. Application of the BFC system to the nozzle flow study has greatly enhanced the capability of the flowfield program to solve problems which hitherto have not been extensively studied. The emphasis of the study has been placed on one- and two-phase inviscid flow in the transonic region. Various particle sizes and particle mass fractions have been investigated in the two-phase flow.

Governing Equations

Normalized by the gas-phase stagnation state corresponding to the condition at the inlet plane, the governing equations written in weak conservative form for an unsteady-state two-phase flow take the following form:

$$\frac{\partial \tilde{E}}{\partial t}+\frac{\partial \tilde{F}}{\partial x}+\frac{\partial \tilde{G}}{\partial r}+\tilde{H}=0 \tag{1}$$

where

$$\tilde{E}=\begin{bmatrix} r^{\delta}\rho \\ r^{\delta}\rho u \\ r^{\delta}\rho v \\ r^{\delta}e \\ r^{\delta}\rho_j(N-1) \\ r^{\delta}\rho_j u_j(N-1) \\ r^{\delta}\rho_j v_j(N-1) \\ r^{\delta}h_j(N-1) \end{bmatrix}, \quad \tilde{F}=\begin{bmatrix} r^{\delta}\rho u \\ r^{\delta}(\tau p+\rho u^2) \\ r^{\delta}\rho uv \\ r^{\delta}[e+(\gamma-1)p]u \\ r^{\delta}\rho_j u_j(N-1) \\ r^{\delta}\rho_j u_j^2(N-1) \\ r^{\delta}\rho_j u_j v_j(N-1) \\ r^{\delta}h_j u_j(N-1) \end{bmatrix}$$

$$\tilde{G}=\begin{bmatrix} r^{\delta}\rho v \\ r^{\delta}\rho uv \\ r^{\delta}(\tau p+\rho v^2) \\ r^{\delta}[e+(\gamma-1)p]v \\ r^{\delta}\rho_j v_j(N-1) \\ r^{\delta}\rho_j u_j v_j(N-1) \\ r^{\delta}\rho_j v_j^2(N-1) \\ r^{\delta}h_j v_j(N-1) \end{bmatrix}, \quad \tilde{H}=\begin{bmatrix} 0 \\ r^{\delta}\rho_j A_j(u-u_j)(N-1) \\ r^{\delta}\rho_j A_j(v-v_j)(N-1)-\delta\tau p \\ r^{\delta}\rho_j A_j B_j(N-1) \\ 0 \\ -r^{\delta}\rho_j A_j(u-u_j)(N-1) \\ -r^{\delta}\rho_j A_j(v-v_j)(N-1) \\ -r^{\delta}\rho_j A_j B_j(N-1) \end{bmatrix}$$

with friction term

$$A_j=\frac{9}{2}\frac{\bar{\mu}_g f_j}{\bar{m}_j \bar{r}_j^2}\frac{\bar{L}}{\bar{V}_{max1}} \tag{2}$$

and energy exchange term

$$B_j=2\gamma[\vec{q}_j\cdot\Delta\vec{q}_j-g_c(T_j-T)-g_r(\epsilon_j T_j^4-\epsilon T^4)] \tag{3}$$

where

$$g_c=Nu_j/6f_jPr$$

$$g_r=\bar{\sigma}\bar{r}_j\bar{T}_{t1}^3/3\bar{c}_p\bar{\mu}_g f_j$$

$$\vec{q}_j\cdot\Delta\vec{q}_j=u_j(u-u_j)+v_j(v-v_j)$$

The momentum transfer parameter f_j is defined as

$$f_j=C_D/C_{D_{Stokes}} \tag{4}$$

where C_D is the drag coefficient based on Henderson's correlating equation[9] for spheres in continuum and rarefied flows, and $C_{D_{Stokes}}=Re_j/24$ is the Stokes law of drag coefficient for spheres in creeping motion.

The heat-transfer parameter, particle Nusselt number, is taken as[10]

$$Nu_j=2+0.459Re_j^{0.55}Pr^{0.33} \tag{5}$$

The particle Reynolds number is based on the relative speed $|\Delta q_j|=|\Delta\vec{q}_j|/\bar{V}_{max1}=\sqrt{(u-u_j)^2+(v-v_j)^2}$ and the particle radius $\bar{r}_j$, and is defined as follows:

$$Re_j=\frac{2|\Delta\vec{q}_j|\bar{r}_j\bar{\rho}}{\bar{\mu}_g}=2|\Delta q_j|\rho\frac{\bar{r}_j}{\bar{\mu}_g}\frac{1}{\tau}\frac{\bar{\rho}_{t1}}{\bar{V}_{max1}} \tag{6}$$

The gas viscosity is evaluated from

$$\bar{\mu}_g=\bar{\mu}_{t1}(\bar{T}/\bar{T}_{t1})^A \tag{7}$$

Numerical Aspects

From a general arbitrary nozzle configuration in the physical plane x,r the transformation to a grid with uniform square mesh in the computational plane ζ,ξ can be accomplished by using BFC; this requires the solution of two elliptical partial differential equations with Dirichlet boundary conditions.[8] The solution utilizing the uccessive over-relaxation (SOR) method for generating the boundary-fitted coordinates is carried out by the TOMCAT program, and the scale factors for transformation are computed in the FATCAT program.[8] The source terms in the TOMCAT program have been turned on to keep the streamwise grid lines near the nozzle wall in the concave region.

Formally applying the chain rule of change of independent variables for Eq. (1) results in the following conservation laws in the ζ,ξ plane:

$$\frac{\partial E}{\partial t}+\frac{\partial F}{\partial \zeta}+\frac{\partial G}{\partial \xi}+H=0 \tag{8}$$

where

$$E=\tilde{E}J_2,\ F=\tilde{F}r_\xi-\tilde{G}x_\xi,\ G=\tilde{F}r_\zeta+\tilde{G}x_\zeta,\ H=\tilde{H}J_2$$

and $J_2=x_\zeta r_\xi-x_\xi r_\zeta$ is the Jacobian of transformation. For a particular nozzle geometry and transformation, the Jacobian and the partial derivatives are computed in the FATCAT program and stored on disk for flowfield study.

The MacCormack finite difference scheme[11] which has been applied successfully to nozzle flow problems[12] is adopted here for the solution of the partial differential Eq. (8).

For one-phase flow, the initial condition is based on a one-dimensional isentropic analysis with the flow vector set to the local inclination angle from linear interpolation between the lower and upper wall slopes along the same grid line (constant ζ). The converged one-phase results serve, then, as the initial guess for the gas-phase data in the two-phase flow.

For the particle-phase arrays of initial velocity lags λ_v and temperature ratios λ_T are chosen, and the initial condition (guess) is

$$\rho_j=\rho\phi/(1-\phi),\quad u_j=u\lambda_v,\quad v_j=v\lambda_v$$

$$T_j=T/\lambda_T,\quad h_j=\gamma\rho_j[\omega T_j+(u_j^2+v_j^2)]$$

A unit velocity lag and temperature ratio as an initial guess of particle phase are satisfactory for this study.

The exit boundary condition is based on a simple linear extrapolation of conservative variables in $\tilde{E}$ of Eq. (1), since the mixture flow is assumed to be supersonic at the exit plane, and the error generated from the extrapolation is not expected to propagate back and affect the upstream results.

The inlet boundary condition for horizontal inflow is computed from a characteristics formulation similar to that of Ref. 1, which provides a fairly smooth subsonic flow in the physical domain. For radial inflow, e.g., the inertial upper stage (IUS) solid rocket motor studied herein, the experimentally evaluated propellant burning rate and chamber pressure/temperature data supply needed information at the propellant burning surface, and a linear interpolation for smoothing flow variables at the grid line adjacent to the propellant burning surface is required to avoid instability in the inlet region.

For a nozzle with a centerbody, the flow variables at the boundary are obtained from linear extrapolation of the data from two adjacent interior points and then modified by the local tangency condition. Without the centerbody in the axisymmetric nozzle, the flow variables take undetermined form at the centerline. The standard L'Hospital rule with the symmetry consideration is used to evaluate all the physical flow variables except the radial velocity, which is zero at the singular centerline. Also, if notice is taken that all the conservative variables at the centerline are zero except $\tilde{H}_3=-\tau p$ (i.e., no restriction is imposed on the gas pressure change at the centerline), a smoothing process involving a linear interpolation for resetting the gas-phase radial velocity v at the first interior point above the centerline is found helpful in stabilizing the solution.

It is important to retain the fourth-order damping terms to the second-order MacCormack finite difference scheme for the unsteady-state application in order to eliminate the nonlinear instability. The formulation adopted here is similar to that of Ref. 13 with a damping coefficient equal to 0.01.

The integration step size is determined by the following expressions:

$$\Delta t=\min\frac{\Delta\ell}{q+a} \tag{9}$$

where

$$\Delta\ell=\sqrt{(\Delta x)^2+(\Delta r)^2}$$

Nozzle with Small Throat Radius of Curvature—JPL Nozzle

One-Phase Flow

The compressible flow inside the JPL axisymmetric nozzle[14] with 45 deg entrance and 15 deg exit straight wall tangent to a circular throat (with ratio of throat radius of curvature to throat height = 0.625) provides a classic comparison for the present nozzle flow study. Figure 1 shows the physical grid generated from the boundary-fitted coordinates system mentioned above. The computed Mach number distributions along the wall and along the centerline are illustrated in Fig. 2; the test data are also shown for comparison. The theoretical gas-only, one-phase result from this study agrees very well with the test data in the entire subsonic-transonic-supersonic flow region. This can be attributed to the good resolution of the boundary flow variables through the use of boundary-aligned grid arrangement. The recompression waves in the supersonic region, which necessarily occur due to overexpansion of the flow near the wall downstream of the throat with small radius of curvature, eventually coalesce into an oblique shock wave near the centerline in the far downstream region. This flow behavior has been observed in test.[1]

The convergence criterion used in all the calculations shown herein requires differences less than 0.01% in Mach number and 0.001% in mass flow rate at the throat for three consecutive time integration steps. For the JPL nozzle with

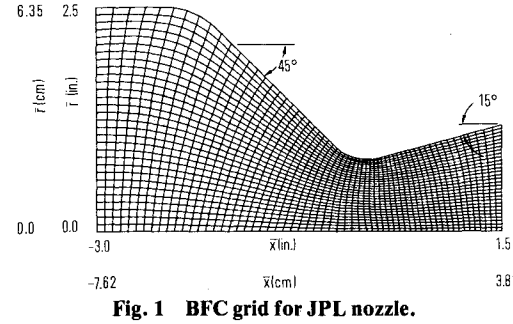

Fig. 1 BFC grid for JPL nozzle.

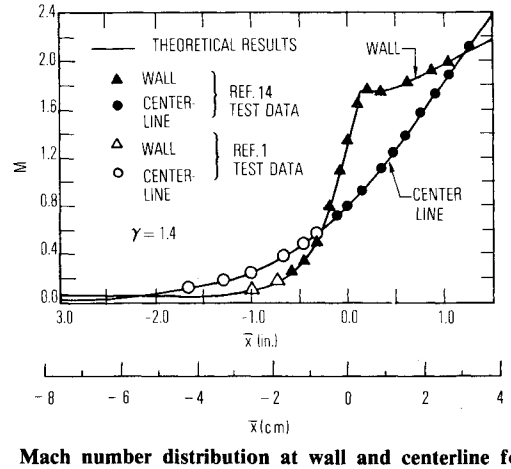

Fig. 2 Mach number distribution at wall and centerline for JPL nozzle (one-phase flow).

61×31 grid points, the converged solution requires 623 integration steps and takes 6 min, 17 s execution time on the CDC 7600 computer. The theoretical results agree well with the test data, thus encouraging further application of the computer code to other nozzle configurations.

Two-Phase Flow

The same flowfield program is applied to the fully coupled, gas-particle, two-phase nozzle flow with the two-phase index N in Eq. (1) set to 2. For the two-phase flow calculation the data shown in Table 1 are adopted. The chamber condition is taken to be $\bar{T}_{tl} = 555.56$ K (1000°R), $\bar{P}_{tl} = 1034.2$ kPa (150 psia). Also, $\epsilon_j = 0.1$ and $\epsilon = 0.05$ are used for the radiative heat exchange between the gas and spherical particles.

The previously computed one-phase flow result is taken as the initial guess for the two-phase flow. Figure 3 shows the computed wall and centerline gas-phase Mach number distribution for various particle sizes with the same $W_j/W_m = 30\%$. While lower gas speed is observed both on the wall and centerline in the two-phase flowfield than that in the gas-only one-phase, the small-sized particles act more effectively to slow down the gas-phase expansion than that of large-sized particles for the same particle mass fraction. This is physically correct, since for the same particle mass fraction the total particle surface area effective for momentum and energy exchange between gas and particles is greater in a two-phase flowfield involving smaller diameter particles.

The effect of different particle sizes in the two-phase flow can be visualized best by comparison of the calculated particle density contour for the small ($\bar{r}_j = 1\ \mu$) and the large ($\bar{r}_j = 20\ \mu$) particles depicted in Fig. 4. For the flow with 1 μ radius particles a sharp change in particle density is obtained near the upper wall downstream of the throat, and the particle density drastically decreases to a small value. But it does not vanish exactly at the wall. With the large ($\bar{r}_j = 20\ \mu$) particle flow, however, a distinctive particle-free zone appears in the calculated result. Since the heavier particles cannot effectively turn around the throat corner with small throat radius of curvature and tend to cluster near the centerline, there are essentially no particles present near the wall downstream of the throat to slow down the gas expansion. This explains why in Fig. 3 the difference between the Mach numbers in one-phase and in large particle two-phase flows near the nozzle lip region is virtually nil, but not so at the exit centerline region.

The computed gas-phase Mach number along the wall and along the centerline for different particle mass fraction W_j/W_m at a given particle radius $\bar{r}_j = 1\ \mu$ is indicated in Fig. 5. It is obvious from these figures that a reduction of particle mass fraction immediately reduces the two-phase "drag" effect. A high particle mass fraction ($W_j/W_m \geq 45\%$) produces an entirely subsonic flow at the geometric throat for the nozzle geometry considered. It is then possible to adjust the exit Mach number from supersonic all the way down to subsonic by varying the particle mass fraction and/or the particle size.

Care must be taken in the case of large particle mass fraction flows ($W_j/W_m > 45\%$) and very small-sized particle flows ($\bar{r}_j < 0.5\ \mu$) in starting from the one-phase initial guess. A sharp drop in the wall Mach number at or near downstream of throat can be expected, especially when the throat radius of curvature is small, necessitating the use of a small time marching step at the beginning of the two-phase calculation. Furthermore, the possibility of subsonic flow occurring at the exit plane requires modification of the supersonic downstream boundary condition or the extension of the exit boundary to a farther downstream location.

Figure 6 summarizes several Mach number contours, $M = 0.1$, 0.2, 0.5, 1.0, and 1.5, for various particle sizes at a fixed ratio $W_j/W_m = 30\%$, and Fig. 7 is the similar result for various particle mass flow ratios at a fixed radius $\bar{r}_j = 1\ \mu$.A typical two-phase run involving 300 integration steps takes approximately 7 min execution time on the CDC 7600 computer.

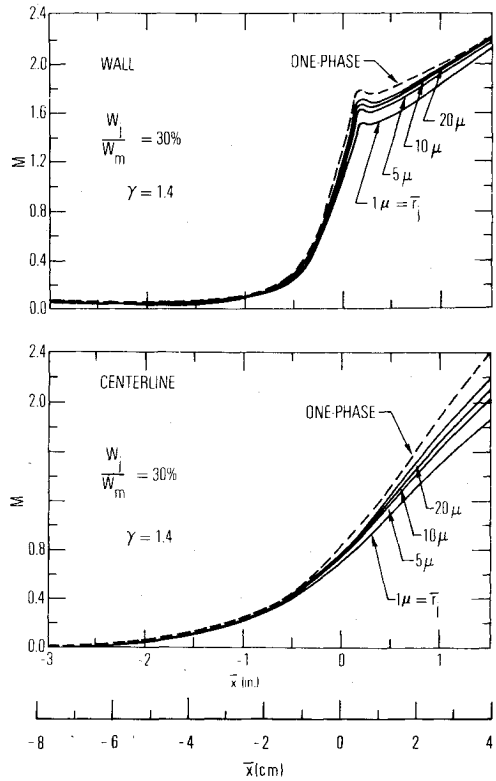

Fig. 3 JPL nozzle Mach number distribution at wall and centerline (two-phase flow $W_j/W_m = 30\%$).

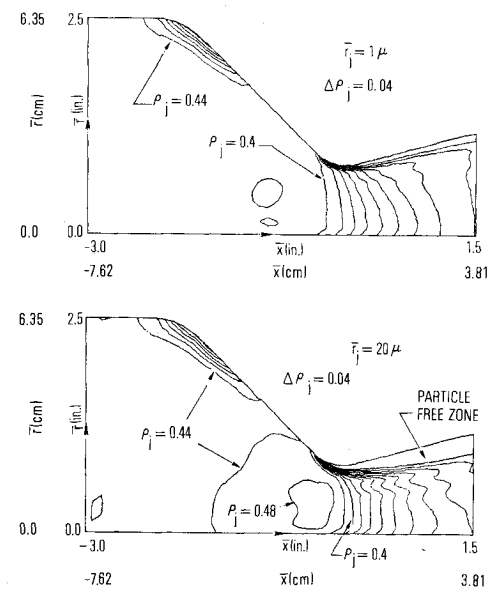

Fig. 4 Particle density contour for $\bar{r}_j = 1\ \mu$ and 20 μ (two-phase flow $W_j/W_m = 30\%$).

Nozzle with Very Steep Entrance—Titan III Motor

One-Phase Flow

A severe test of the present numerical technique is the solution of the compressible flowfield inside a nozzle with near vertical entrance region shown in Fig. 8, which also illustrates the grid generated from the boundary-fitted coordinates system. The nozzle steep entrance contour is that of the Titan III solid rocket motor nozzle. The specific heat for the combustion products is $\gamma = 1.19$. The computed wall and centerline Mach number distribution is given in Fig. 9. The same nozzle was analyzed with $\gamma = 1.4$, and the results are also plotted on the same figure which serves to illustrate the effect of different γ on the Mach number distribution. The

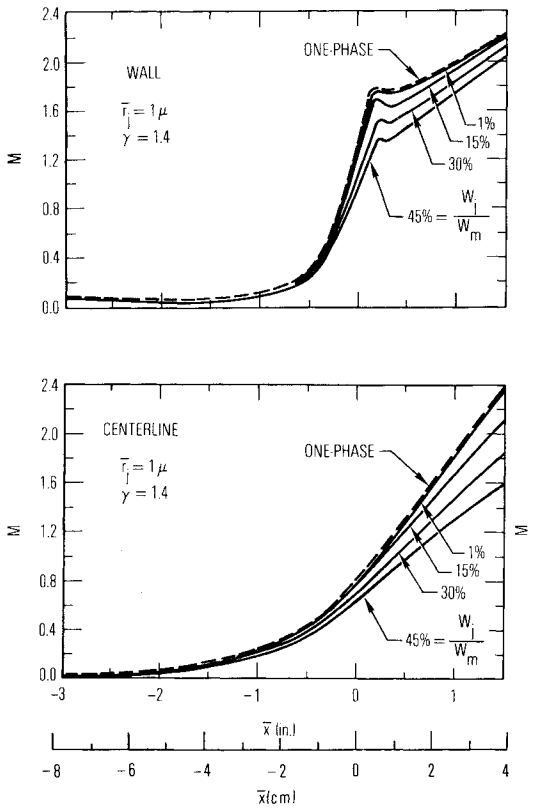

Fig. 5 JPL nozzle Mach number distribution at wall and centerline (two-phase flow $\bar{r}_j = 1\,\mu$).

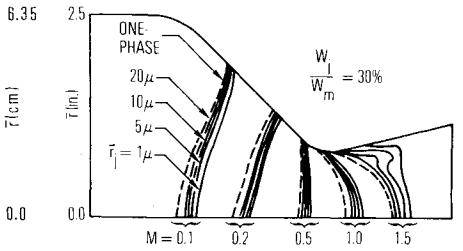

Fig. 6 Mach number contours for different particle sizes (two-phase flow $W_j/W_m = 30\%$).

converged one-phase flow solution for $\gamma = 1.19$ requires 890 integration steps and takes 8 min, 58 s on the CDC 7600 computer. Figure 10 is the Mach number contour plot. The sonic point on the wall has been observed to be far upstream of the throat, which indicates that higher heating rate occurs farther upstream of the throat than that expected from the simple one-dimensional analysis. This partially explains why, in past full-scale firings, the Titan III motor nozzle was ablated much more in a region far upstream of the throat than at the throat. Cold-flow tests were recently conducted at the Chemical Systems Division of United Technology Corporation for the 6 deg canted Titan III solid rocket motor using nitrogen with $\gamma = 1.4$; the wall Mach number at the throat was measured[15] to be 1.52, which agrees fairly well with the computed value 1.6 for the axisymmetric nozzle.

No converged solution is possible with the conventional grid with vertical axial stations, such as that used in Ref. 1 and in most of the nozzle studies reported thus far,[2] for the nozzle with a steep wall slope like that of the Titan III motor. It is the author's experience that when the nozzle wall slope is greater than ≈ 60 deg, the conventional grid with vertical axial station cannot handle the drastic change in flow properties along the steep wall, and that this results in numerical instability. On the contrary, no difficulty is encountered in the calculation with the grid generated from the boundary-fitted coordinates system.

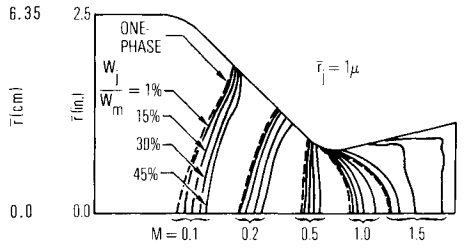

Fig. 7 Mach number contours for different particle mass fractions (two-phase flow $\bar{r}_j = 1\,\mu$).

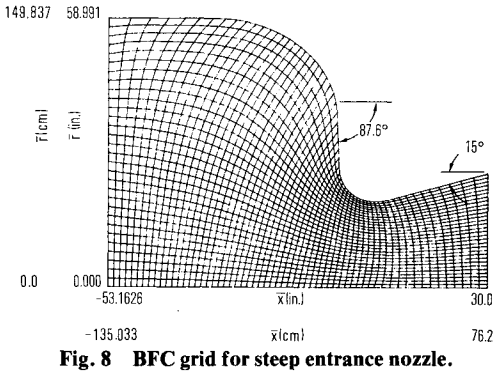

Fig. 8 BFC grid for steep entrance nozzle.

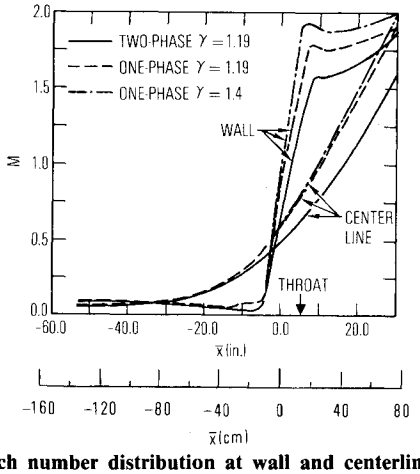

Fig. 9 Mach number distribution at wall and centerline for steep entrance nozzle.

Two-Phase Flow

The two-phase flow data for the Titan III motor are shown in Table 1. The chamber condition is $\bar{T}_{tl} = 3272$ K (5890°R), $\bar{P}_{tl} = 4136.9$ kPa (600 psia).

The gas-phase Mach number distribution is shown in Fig. 9 for comparison with that of one-phase flow and Mach number contour is plotted in Fig. 10. The particle density contour is depicted in Fig. 11. The calculation of 500 integration steps for the two-phase flow takes 10 min, 37 s execution time on the CDC 7600 computer.

Particles are likely to impinge on the steep wall in the entrance region. The present analysis does not incorporate any pertinent particle impingement model for calculating either the erosion or particle energy transfer caused by such impingement. Nevertheless, the particle density contour obtained from this study does show regions of high particle concentration which may affect the results from boundary-layer calculations and thereby the results of transient in-depth thermal analyses for the prediction of nozzle wall temperature.

Table 1 Two-phase flow data for various nozzles

Nozzle	Gas phase	Particle phase
JPL	$\bar{C}_p = 1.07$ kJ/kg-K (0.255 Btu/lbm-°R) $\bar{\mu}_{tl} = 2.68 \times 10^{-5}$ Pa·s (1.8×10^{-5} lbm/ft-s) $\gamma = 1.4$ $Pr = 0.74$ $A = 0.6$	$\bar{C}_j = 1.38$ kJ/kg-K (0.33 Btu/lbm-°R) $\bar{m}_j = 4004.62$ kg/m^3 (250 lbm/ft^3)
Titan III	$\bar{C}_p = 2.68$ kJ/kg-K (0.64 Btu/lbm-°R) $\bar{\mu}_{tl} = 8.88 \times 10^{-5}$ Pa·s (5.97×10^{-5} lbm/ft-s) $Pr = 0.45$ $A = 0.664$ $\gamma = 1.19$	$\bar{C}_j = 1.38$ kJ/kg-K (0.33 Btu/lbm-°R) $\bar{m}_j = 3203.69$ kg/m^3 (200 lbm/ft^3) $r_j = 6\,\mu$ $W_j / W_m = 28.8\%$
IUS	$\bar{C}_p = 1.88$ kJ/kg-K (0.45 Btu/lbm-°R) $\bar{\mu}_{tl} = 8.444 \times 10^{-5}$ Pa·s (5.67×10^{-5} lbm/ft-s) $Pr = 0.269$ $A = 0.65$ $\gamma = 1.19$	$\bar{C}_j = 1.34$ kJ/kg-K (0.32 Btu/lbm-°R) $\bar{m}_j = 3203.69$ kg/m^3 (200 lbm/ft^3) $W_j / W_m = 30\%$ $\bar{r}_j = 2.5\,\mu$

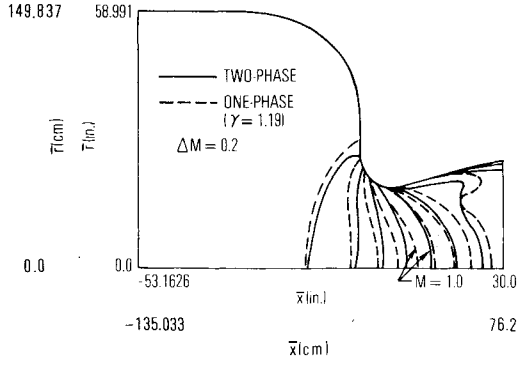

Fig. 10 Mach number contour for steep entrance nozzle.

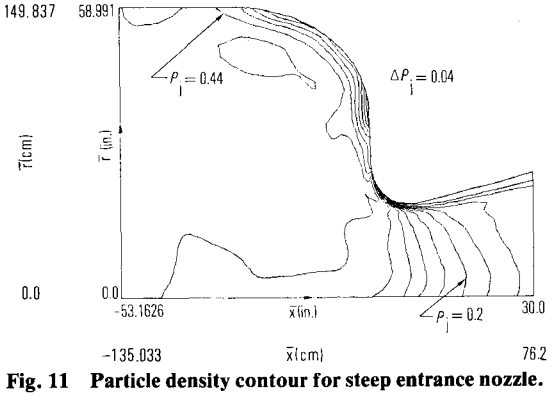

Fig. 11 Particle density contour for steep entrance nozzle.

Submerged Nozzle—IUS Small Motor

One-Phase Flow

It has long been recognized that the solution of the flowfield inside rocket motors with a submerged nozzle configuration constitutes an important phase of the flowfield study. Both large and small IUS solid rocket motors have a submerged nozzle. Although the viscous effect would probably dominate some part of the submerged flow region in the gas-only, one-phase flow, the inviscid flow solution shown here constitutes a first attempt toward a complete viscous flow solution in future studies.

The IUS small motor interior geometry including the igniter, submerged nozzle block, and a propellant burning surface is illustrated in Fig. 12, where the physical region for computation has been identified by heavy solid lines. The grid

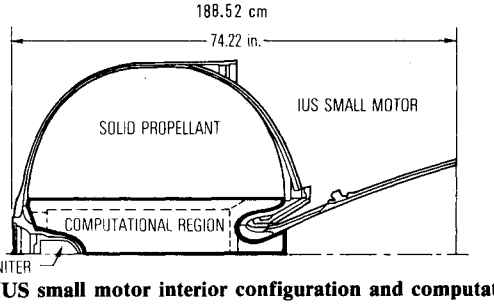

Fig. 12 IUS small motor interior configuration and computational region.

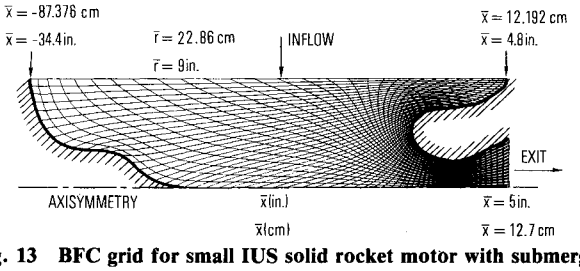

Fig. 13 BFC grid for small IUS solid rocket motor with submerged nozzle block.

generated from the boundary-fitted coordinates system is depicted in Fig. 13. The region depicted in Fig. 13 incorporates the entire subsonic flow region without introducing a fictitious vertical inlet boundary.

The propellant burning rate for the small IUS solid rocket motor is 0.5232 cm/s (0.206 in./s) at $\bar{T}_{tl} = 3325$ K (5985°R), and $\bar{P}_{tl} = 2826.9$ kPa (410 psia), which results in the fixed inlet condition at the propellant burning surface $\bar{v} = 3.5143$ m/s (11.53 ft/s) ($M = 0.00322$) for $\bar{C}_p = 1.88$ kJ/kg-K (0.45 Btu/lbm-°R) and $\gamma = 1.19$. In this paper, the boundary points with the radial coordinate smaller than the radial length of the adjacent finite-difference mesh are treated as the centerline points of zero radius and L'Hospital rule is conveniently applied, thereby avoiding numerical error resulting from decoding conservative variables divided by a very small number (small radial coordinate).

Unlike the previous two nozzle flows, a more strict convergence criterion is deemed necessary for the submerged nozzle calculation and requires that the difference in Mach number and in mass flow rates be less than 0.001% at the throat for three consecutive integration steps. For the 61×31 grid points shown in Fig. 13, the converged solution requires 4487 integration steps and takes 38 min, 16 s execution time on the CDC 7600 computer.

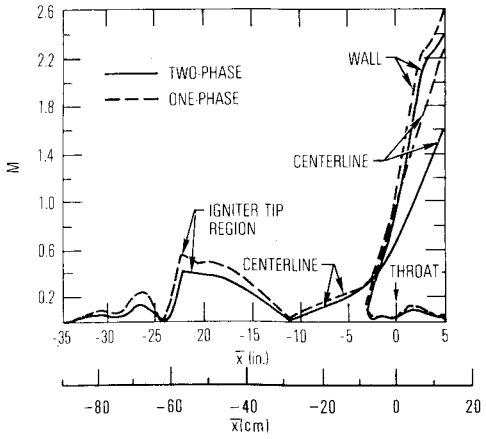

Fig. 14 Mach number distribution on boundary for small IUS nozzle.

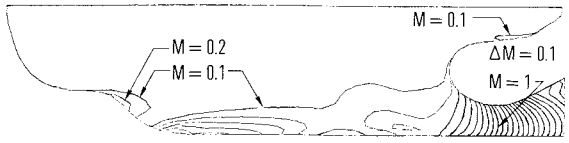

Fig. 15 Mach number contour for small IUS (one-phase flow).

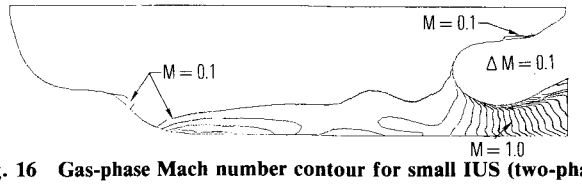

Fig. 16 Gas-phase Mach number contour for small IUS (two-phase flow).

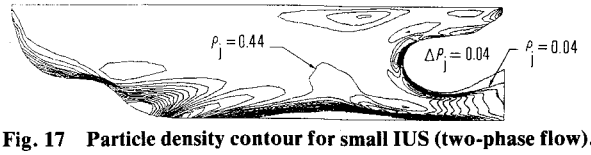

Fig. 17 Particle density contour for small IUS (two-phase flow).

The IUS solid rocket motor has a throat with a large radius of curvature; the computed Mach number at the throat is 1.071 on the wall and 0.947 at the centerline which are close to a uniform one-dimensional flow. Figure 14 depicts the Mach number distribution along the boundary, while the computed Mach number contour is plotted in Fig. 15.

Two-Phase Flow

The data used for the two-phase flow inside the small IUS motor are listed in Table 1. The chamber condition is $\bar{T}_{tl} = 3325$ K (5985°R), $\bar{P}_{tl} = 2826.9$ kPa (410 psia).

The Mach number distribution along the boundary surface is indicated in Fig. 14. The gas-phase Mach number at exit plane is 1.57 at centerline and 2.41 at wall for the two-phase flow; these are smaller than the corresponding Mach numbers of 2.25 and 2.57 found in the gas-only, one-phase flow. This implies that an IUS solid rocket motor nozzle flowfield and heat-transfer analysis based solely upon a gas-only one-phase study will be in error. Figure 16 is the computed gas-phase Mach number contour, and Fig. 17 is the particle density contour in the two-phase flow.

Although the submerged nozzle configuration is complex and the governing two-phase partial differential equations are highly nonlinear, no computational difficulty has been encountered during the course of this study, and the timewise integration has been carried out in a straightforward manner. For the submerged small IUS solid rocket motor nozzle, the two-phase flowfield calculation of 1000 integration steps takes 23 min, 2 s execution time on the CDC 7600 computer. All the two-phase flow features mentioned previously for the JPL and Titan III nozzle are equally applicable to this submerged IUS solid rocket motor nozzle.

Conclusions

The following conclusions have been reached as a result of this study:

1) A time-dependent technique with the MacCormack finite-difference scheme provides stable integration for both one- and two-phase nozzle flow equations.

2) The utilization of the BFC system enhances the capability of the program to the solution of flow inside nozzles with complex geometry.

3) Recompression region can occur near the wall of the nozzle geometric throat for the flow inside nozzle with small throat radius of curvature.

4) The small-sized particles act more effectively to slow down the gas-phase expansion than that of large-sized particles for the same particle mass fraction.

5) For a two-phase flow with high particle loading ratio, the gas phase can become subsonic at the geometric throat.

6) The computed one- and two-phase results are important for nozzle wall heat transfer and ablation study.

7) In general, the assumption of constant fractional lag is not justified for a two-phase transonic flow. The prediction of the gas-particle flowfield requires that the proper momentum and energy exchange between the gas and particles, such as the fully coupled solution presented in this study, be taken into account.

Acknowledgments

The author wishes to express his gratitude to the late Dr. John Vasiliu for his review of this paper and for his encouragement and helpful suggestions throughout the study. This research was supported by the Air Force Space Division under Contract F04701-79-C-0080.

References

[1] Serra, R. A., "Determination of Internal Gas Flows by a Transient Numerical Technique," *AIAA Journal*, Vol. 10, May 1972, pp. 603-611.

[2] Brown, E. F. and Hamilton, G. L., "A Survey of Methods for Exhaust-Nozzle Flow Analysis," AIAA Paper 75-60, 1975.

[3] Hoglund, R. F., "Recent Advances in Gas-Particle Nozzle Flows," *ARS Journal*, May 1962, p. 662.

[4] Regan, J. F., Thompson, H. D., and Hoglund, R. F., "Two-Dimensional Analysis of Transonic Gas-Particle Flows in Axisymmetric Nozzles," *Journal of Spacecraft and Rockets*, Vol. 8, April 1971, p. 346.

[5] Jacques, L. J. and Seguin, J.A.M., "Two-Dimensional Transonic Two-Phase Flow in Axisymmetric Nozzles," AIAA Paper 74-1088, Oct. 1974.

[6] Kliegel, J. R. and Nickerson, G. R., "Axisymmetric Two-Phase Perfect Gas Performance Program," TRW Systems Group, Redondo Beach, Calif., Rept. 02874-6006-R0000, Vols. I and II, April 1967.

[7] Coats, D. E., et al., "A Computer Program for the Prediction of Solid Propellant Rocket Motor Performance," AFRPL-TR-75-36, Vols. I, II, and III, July 1975.

[8] Thompson, J. F., Thames, F. C., and Martin, C. W., "Boundary-Fitted Curvilinear Coordinates Systems for Solution of Partial Differential Equations on Fields Containing Any Number of Arbitrary Two-Dimensional Bodies," NASA CR 2729, July 1977.

[9] Henderson, C. B., "Drag Coefficients of Spheres in Continuum and Rarefied Flows," *AIAA Journal*, Vol. 14, June 1976, p. 707.

[10] Carlson, D. J. and Hoglund, R. F., "Particle Drag and Heat Transfer in Rocket Nozzles," *AIAA Journal*, Vol. 2, Nov. 1964, p. 1980.

[11] MacCormack, R. W., "The Effect of Viscosity in Hypervelocity Impact Cratering," AIAA Paper 69-354, May 1969.

[12] Chang, I-Shih, "Three-Dimensional Supersonic Internal Flows," AIAA Paper 76-423, July 1976.

[13] Kutler, P., Sakell, L., and Aiello, G., "On the Shock-on-Shock Interaction Problem," AIAA Paper 74-524, June 1974.

[14] Cuffel, R. F., Back, L. H., Massier, P. F., "Transonic Flowfield in a Supersonic Nozzle with Small Throat Radius of Curvature," *AIAA Journal*, Vol. 7, July 1969, p. 1364.

[15] Dunlop, R., private communication, Chemical Systems Div., United Technology Center, Nov. 1978.